Chem Soc Rev

Exchange-coupled Nanocomposites: Chemical Synthesis, Characterization and Applications

Journal:	*Chemical Society Reviews*
Manuscript ID:	CS-REV-05-2014-000162.R2
Article Type:	Review Article
Date Submitted by the Author:	29-Jul-2014
Complete List of Authors:	Liu, Fei; Peking University, College of Engineering Hou, Yanglong; Peking University, College of Engineering Gao, Song; Peking University, State Key Lab. of Rare Earth Materialds Chemistry

Journal Name

RSCPublishing

ARTICLE

Exchange-coupled Nanocomposites: Chemical Synthesis, Characterization and Applications

Cite this: DOI: 10.1039/xOxxOOOOOx

Fei Liu,[a] Yanglong Hou[a] and Song Gao[b]

Received 00th January 2012,
Accepted 00th January 2012

DOI: 10.1039/xOxxOOOOOx

www.rsc.org/

Nanocomposites containing soft and hard magnetic phases have attracted immense attention for energy-related and biomedical applications. With exchange coupling between nanoscale grains in the composites, magnetization of the soft magnetic phase can rotate coherently with that of the hard magnetic phase. In particular, good control of the soft and hard phases at the nanoscale in the composites is of great importance for effective exchange coupling, allowing us to make the best of the strengths of soft and hard magnetic phases and to optimize the magnetic properties for targeted applications. In this review, we present recent progress in chemical synthesis and applications of exchange-coupled nanocomposites. Firstly, the principle of nanomagnetism and exchange coupling is introduced. Secondly, the characterizations of exchange-coupled nanocomposites are summarized. Thirdly, the chemical methods for different exchange-coupled nanocomposites are presented. Finally, applications of exchange-coupled nanocomposites in magnetic energy storage and biomedicine are addressed.

Introduction

Functional magnetic materials are ubiquitous in human life. In the contemporary society, magnetic materials have been widely used in a variety of applications especially energy-related applications such as electric motors, generators and transformers.[1] With the growing concerns for energy and environment, research into energy-related technologies has been accelerated. One key issue is to improve the energy efficiency and performance of the devices. For devices utilizing permanent magnetic materials as components, such improvements demand maximized energy product of the permanent magnets which enable miniaturization of the devices, and therefore, the consumption of electrical power in operating the devices can be effectively reduced. Over the past century, energy product of the permanent magnets have been significantly improved by searching for new compounds.[2-5] The successive discovery of hard magnetic materials from hexagonal ferrites $BaFe_{12}O_{19}$ to rare-earth (RE) transition-metal intermetallic compounds $SmCo_5$ and $Nd_2Fe_{14}B$ enables the enhancement of energy product by two orders of magnitude, reaching a peak at ~56 MGOe for Nd-Fe-B magnets. Owing to high energy product and relatively low cost, Nd-Fe-B magnets have captured a large percentage of the world market share for permanent magnets.[1] However, the REs, especially those heavy ones, such as Dy and Tb used in Nd-Fe-B magnets for maintaining superior performance at elevated temperature are very expensive and not sustainable.[6, 7] Seeking a new compound to replace Nd-Fe-B magnets might be an alternative to solve this problem, but research encountered the bottleneck in the past decades. On the other hand, advanced permanent magnets with even better performance than Nd-Fe-B magnets are still demanded. Thus, finding a new approach to design and develop permanent magnets with reduced RE content and/or enhanced energy product is becoming important and urgent.

When the size of the magnetic materials is down to the nanoscale, new types of magnetic behavior appear. This size effect will result in single domain ferromagnetic and superparamagnetic (SPM) nanoparticles (NPs), which have attracted intensive interest recently due to their extraordinary potential for magnetic energy storage and biomedical applications.[8-13] Ferromagnetic NPs will reach a maximum coercivity at a critical size, so they are promising as building blocks for the fabrication of high-energy product permanent magnets and high-density recording film.[14, 15] In addition, superparamagnetic NPs with their ability to respond to external magnetic fields have been demonstrated to show great promise in cancer diagnosis and therapy, i.e. drug delivery, magnetic resonance imaging and magnetic hyperthermia.[16-18] To fully

exploit the nanoscale effects and realize optimum property for targeted applications, the understanding of nanomagnetism, control of magnetic properties and development of related synthetic methods are of great importance.

The discovery of exchange coupling in the composites consisting of soft and hard magnetic phases has brought a novel approach not only for producing high-energy product permanent magnets but also for tuning magnetic properties of NPs. To realize effective exchange coupling, the size of the soft phase should be carefully manipulated.[19-21] The soft and hard phases will reverse independently if the size of soft phase is sufficiently large. However, when the soft phase reduces its size to about twice the domain wall width of the hard phase, magnetic moments of both phases will be switched coherently as if a single magnetic phase is present. In particular, chemical method offers an effective route to precisely control both phases at the nanoscale, allowing rational tuning of the composition for effective exchange coupling and optimal magnetic performance. In addition, chemical tool opens up corridors for understanding of magnetic interactions at the nanoscale and developing advanced magnetic materials for various applications.

In this review, we aim to provide an overview of recent developments related to chemical synthesis and applications of exchange-coupled nanocomposites. The review first introduces the general principles of nanomagnetism and exchange coupling, and outlines several ways for characterization of exchange coupling. It then discusses chemical synthesis of exchange-coupled nanocomposites divided by the types of the hard magnetic component. Toward the end, the potential applications of the exchange-coupled nanocomposites in energy storage and biomedicine are highlighted.

General principles

The magnetization curve (Fig. 1a) that measures the change of magnetic moment (M) over the strength of an applied magnetic field (H) can be generally used to understand the magnetic behavior of ferro- and ferrimagnetic materials. From the magnetization curve, the key parameters such as coercivity (H_c), saturation magnetization (M_s) and remanent magnetization (M_r) can be easily derived to describe the magnetic property of the materials. For a soft magnet, the magnetization can be readily saturated in a weak field, leading to a very small coercive field to bring the net magnetization back to zero. While for a hard magnet, there is an obvious hysteresis in the magnetization curve, and the required coercive field is far stronger than that of the soft magnet.

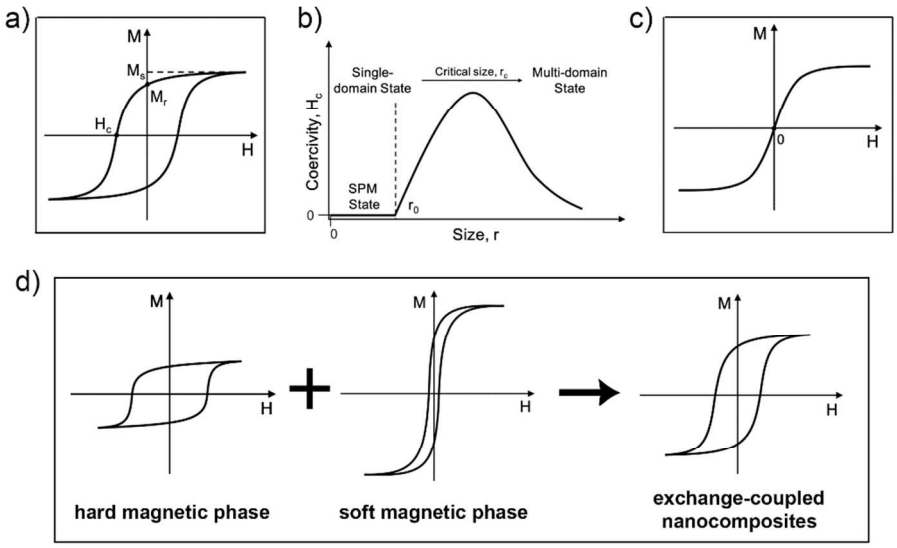

Fig. 1. a) A typical hysteresis loop of a ferro- or ferrimagnetic material. b) Schematic illustration of the dependence of coercivity on particle size. c) A typical hysteresis loop of a SPM material. d) Exchange coupling between hard and soft magnetic phases.

The magnetism of ferro- and ferrimagnetic materials are highly volume dependent (Fig. 1b). To minimize the magnetostatic energy, the bulk magnet always possesses multiple magnetic domain structures. When the size (r) decreases to a certain critical value, the energy for creating a domain wall becomes larger than the external magnetostatic energy, and therefore, the single-domain state appears. The critical size r_c of a spherical particle, at which there is a transition from multi-domain state to single-domain state, can be described as $r_c = \frac{36\sqrt{AK}}{\mu_0 M_s}$, where A is the exchange constant, K is the effective anisotropy constant and μ_0 is the vacuum permeability. In the single-domain state, coercivity is size dependent, and can reach a maximum value at the transition between modes of coherent rotation and curling. With the decrease of the size of single-domain particle to a value r_0, thermal energy becomes large enough to overcome the anisotropy energy for holding the magnetic moments along a certain direction. As a result, the magnetization of an array of such particles can be easily flipped under the influence of temperature. If the time scale of measurement is longer than the relaxation time (the time between two flips), the particles can be magnetized in the presence of an external field, and their magnetization will appear to be in average zero upon removal of the field, similarly to conventional paramagnets. Such a system of particles is referred to be SPM with no hysteresis behavior (both M_r and H_c are zero), and the major difference from the paramagnets is that the magnetic susceptibility (M/H) is much larger. A typical hysteresis loop of a superparamagnetic material is shown in Fig. 1c.

The exchange coupling effect between soft and hard magnetic phases was demonstrated by Coehoorn et al. to explain the remanence enhancement in isotropic $Nd_2Fe_{14}B/Fe_3B$ composite magnets.[22] After that, several groups proposed the concept of exchange-coupled composite magnets,[23-27] demonstrating the possibility to build superstrong permanent magnets. Owing to the artificially constructed magnetic structures, the magnets can attain giant energy product with high magnetization from the soft phase and high magnetic anisotropy from the hard phase. In the early one-dimensional simulation model proposed by Kneller and Hawig,[19] effective exchange coupling requires soft phase layer that is thin enough, thus magnetization direction in both layers can rotate coherently. By using a finite element technique, the critical soft-layer thickness was calculated to be roughly twice the domain wall width of the hard phase.[21] In addition, the property of the soft phase has been found to be essential for the exchange coupling.[28-32] If the anisotropy of the soft phase is considered in the simulation, the critical soft phase dimension will be affected. Soft phase with relatively high anisotropy (like FeCo) will be better for constructing composite magnets since the critical soft phase dimension can be larger. Another important aspect that may determine the exchange coupling between the soft and hard magnetic phases is the interface of two phases. Recent experimental and theoretical investigations showed that the intermixed interface could lead to the great enhancement of the energy product.[33-35] By analyzing the interfacial composition profile and magnetization reversal process, it was suggested that the graded interface was preferred because it could create a region with intermediate anisotropy value which is more resistant to magnetization reversal than "absolutely soft" phase in the case of sharp interface, and thus effective exchange coupling could be acquired.

In spite of playing essential roles in designing and developing superstrong permanent magnets, exchange coupling has also been regarded as an efficient tool to tune the magnetism of nanosystems for various applications. For the NPs comprised of soft and hard magnetic components, the K (or H_c) values of the NPs can be tailored by controlling the magnetic components. According to theoretical study,[23] H_c of the hard-soft exchange-coupled system can be expressed as $H_c = 2\frac{K_H f_H + K_S f_S}{M_H f_H + M_S f_S}$, where f is the volume fraction, and the subscripts H and S denote the hard and soft phases, respectively. The expression can be further simplified as $H_c = \frac{2K_H}{M_H}(1 - f_S)$ in the premise that K_H is much larger than K_S and M_s values of both phases are close. Therefore, the coercivity of the NPs is estimated to be linearly propositional to the volume fraction of the soft phase. Magnetic measurements on FePt and $CoFe_2O_4$-based hard-soft NPs showed good agreement with the simulation.[36, 37] However, H_c of the exchange-coupled NPs can be quite different if the hard phase stays at different position even though the volume fraction of the soft phase is the same. For the 10-nm core/shell NPs constructed by the phases of $CoFe_2O_4$ and $MnFe_2O_4$, Song et al. found that $CoFe_2O_4$ as the shell requires about 3.6 times the volume as it acts as the core to achieve almost the same H_c of ~9.7 kOe.[37] They ascribed such a dramatic difference to the different magnetization switching mechanism of the NPs.

Characterization of exchange coupling

With the development of modern technology, several techniques have been employed to characterize exchange coupling between the components in the nanocomposites, here we will summarize these technologies as follows.

Transmission electron microscopy

Transmission electron microscopy (TEM) has been regarded as one of the most powerful tools for characterizing the structure of magnetic materials including exchange-coupled nanocomposites. Their physical structure such as crystal structure, morphology, grain size, volume fraction of each phase, inter-phase interfaces and etc. can be analyzed by TEM in detail. Owing to the high resolution of TEM, it is possible to identify the individual phase and coherent planes by measuring the lattice fringe distance in different zones in the imaging mode. More information of crystal structure can be deduced from selected area diffraction pattern and fast Fourier transform spots. Furthermore, TEM provides compositional analysis by X-ray energy dispersive spectrometry or energy loss spectroscopy, and therefore, one can readily know the element (or phase) distribution in the nanocomposites. TEM technology is an indirect way for characterization of exchange coupling. When the exchange-coupled nanocomposites are characterized by TEM, the interface between soft/hard magnetic phases is visible and the dimension of the soft phase is in good agreement with the limit for effective exchange coupling according to simulation model.

Magnetization curves

Analyzing the hysteresis loop at room temperature (or at low temperature) is always necessary for any magnetic material. The magnetization curves also offer a reliable and simple way to check exchange coupling between the soft and hard magnetic phases.[19] In case of effective exchange coupling, the hysteresis loop of the nanocomposites will behave like a single magnetic phase without unusual drops, kinks or shoulders that generally originate from superposed loops of the soft and hard magnetic components. In addition, for arrays of particles with randomly oriented easy axes, the value of the remanence ratio that is greater than 0.5 as theoretically predicted by Stoner-Wohlfarth model[38] may also be a manifestation of exchange coupling.

The exchange coupling in the nanocomposites can be further clarified by low temperature measurement.[39] At low temperature, as the anisotropy of the hard magnetic component in the composite is enhanced, the size limit of the soft phase (D) for effective exchange coupling will be decreased according to the equation $D \leq 2\delta = 2\pi\sqrt{\frac{A}{K_H}}$, where δ is the domain wall width of the hard phase. As a result, a decoupling will occur at a certain temperature for initially exchange-coupled nanocomposites when K_H is large enough to give 2δ that is smaller than the size of the soft phase, leading to the appearance of two-step magnetization reversal behavior.

δM method (Henkel plot)

The magnetic interactions in the nanocomposites can be understood via δM method (Henkel plot) by comparing the remanent magnetization of the sample with that in the ideal non-interacting Stoner-Wohlfarth system.[40, 41] The behavior of interactions can be defined as $\delta M = M_d$-(1-2M_r), where M_d is the reduced direct current demagnetization remanence and M_r is the reduced isothermal remanent magnetization. The value of

δM is normalized by the saturation remanence. For the measurement of M_d, the sample is initially saturated in a directly applied field. After the field is removed, a small reverse field is applied and then removed, giving the remanent magnetization. A series of remanent magnetization are measured by repeating the reverse magnetization process with slightly increased reverse field until the sample has reached saturation in the opposite direction. M_r is measured by applying and subsequently removing the magnetic field in the forward direction. In general, δM with positive values can indicate the existence of exchange coupling, whereas interactions such as magnetic dipolar interactions that tend to assist the magnetization reversal will give negative values.[42-44] As seen in Fig. 2, δM of $SmCo_5$/Fe nanocomposites is initially positive, indicating strong inter-phase interactions. It drops from positive to negative values during reversal due to the magnetostatic interactions provided by Fe phase. These behavior in the δM plot may evidence interphase exchange coupling in the $SmCo_5$/Fe nanocomposites.

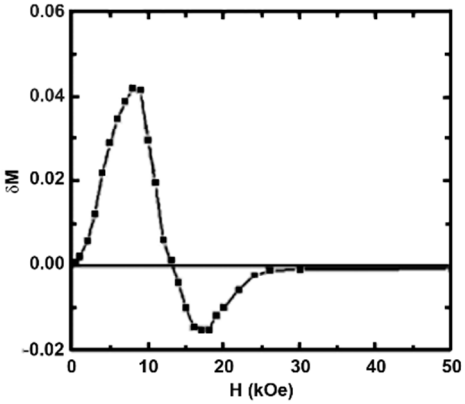

Fig. 2. δM plot of $SmCo_5$/Fe nanocomposites. Reproduced with permission from Ref. 43.Copyright 2007 American Institute of Physics Publishing LLC.

Recoil curves

Recoil curves that result from the removal and re-application of a demagnetizing field can be used to distinguish the exchange-coupled nanocomposites from single-phase magnets because the recoil characteristics are sensitive to interphase interactions.[45, 46] The magnetic sample for the measurement of recoil curves is initially saturated in a directly applied field followed by removing the field. Then the field in the opposite direction is applied and removed alternatively as the demagnetizing field is gradually increased. For a single-phase magnet, the recoil loops are close and flat, indicating the absence of interphase interactions. In contrast, for the exchange-coupled nanocomposites, the magnetizing and demagnetizing branches will encompass a finite area, leading to the open and steep recoil loops. The appearance of open recoil loops at reverse fields that are great enough can be ascribed to the breakdown of exchange coupling, as the decoupled magnetic phases may undergo individual magnetic reversal.

Other methods

There are also a few techniques that are helpful to determine and characterize exchange coupling. The first-order reversal curve (FORC) diagram can be used for analysis of magnetization reversal processes and visualization of exchange coupling.[47, 48] In the FORC diagram for exchange-coupled nanocomposites, there exists only one peak, indicating that the magnetization of two phases switches at the same magnetic field. If the magnetic phases are decoupled, two distribution peaks attributed to independent switching will be observed in low and relatively high coercivity regions. Synchrotron-based X-ray magnetic measurements can give element-specific magnetic hysteresis loops for distinguishing magnetic contributions from individual components in the nanocomposites.[49] Based on the comparison between the element-specific magnetic hysteresis loops and the overall hysteresis loops, the effect of exchange coupling can be deduced. In fact, using multiple characterization methods will enhance the reliability and accuracy for detecting and identifying exchange coupling.

Chemical synthesis of exchange-coupled nanocomposites

Exchange-coupled nanocomposites can be obtained in various forms including bulk shapes, nanoscale shapes and thin films by different approaches. Conventional physical techniques such as melt-spinning, mechanical milling and sputtering have been exploited to fabricate exchange-coupled nanocomposites,[50] however, it is very challenging to control the hard and soft phases at the nanoscale and to achieve uniform phase distribution for effective exchange coupling. Chemical method has been regarded as a highly efficient tool to produce dispersible magnetic materials with controlled sizes, shapes, compositions, components and crystalline/topological structures by tuning the synthetic conditions. In particular, the success made in the synthesis of magnetic NPs offers a novel approach from the bottom to control the nanoscale morphology of soft/hard magnetic phases in the exchange-coupled nanocomposites. In this section, we will overview the progress in the chemical synthesis of exchange-coupled nanocomposites divided by the types of the hard magnetic component, including $CoFe_2O_4$, FePt /FePd, and RE intermetallics.

$CoFe_2O_4$-based nanocomposites

Cobalt ferrite represented by an inverse spinel structure is an important class of conventional ferrimagnetic iron oxides. In the unit cell, O^{2-} anions form the closely packed face-centered cubic (*fcc*) structure and Co^{2+} and Fe^{3+} cations occupy the interstitial sites surrounded by O^{2-} anions. Co^{2+} along with half of the Fe^{3+} cations fill the octahedral interstitial sites, while another half of the Fe^{3+} cations take the tetrahedral interstitial sites, leading to a theoretical magnetic moment of $3\mu_B$. Owing to Co^{2+} cations in the structure, cobalt ferrite is magnetically hard with a large value of K over 10^5 J m^{-3}.

Cobalt ferrite NPs can be prepared by the decomposition of metal precursors in the high-boiling-point solvent in the presence of surfactants.[51-55] For example, using a stoichiometric amount of cobalt(II) acetylacetonate, $Co(acac)_2$ and $Fe(acac)_3$ with 1,2-hexadecanediol, oleic acid, and oleylamine, Sun et al. produced monodisperse $CoFe_2O_4$ NPs with the tunable size of 3 to 20 nm by varying the reaction temperature or using a seed-meditated growth process.[55] In the improved synthesis, 1,2-hexadecanediol was removed from the reaction, and $CoFe_2O_4$ NPs with the size from 7 to 50 nm could be prepared.[52] Oleic acid and oleylamine involved in the reaction were found to be

essential for size and morphology control of the NPs. As a result, the cobalt ferrite NPs with the size of 35 nm have a coercivity over 1 kOe at room temperature, and can be further tuned by controlling the molar ratio between Fe and Co in the NPs.

Replacing Co^{2+} with other metal cations (Fe^{2+}, Mn^{2+}, Ni^{2+}, etc.) in the spinel structure can result in the soft magnetic ferrites with much reduced *K*. These soft magnetic ferrites have the same crystallographic structure and almost negligible lattice mismatch with cobalt ferrite, and therefore, it is feasible to establish exchange-coupled platform through an epitaxial growth approach. Choosing cobalt ferrites or other soft magnetic ferrites as starting materials, core/shell architecture with markedly controllable and uniform core and size dimensions can be acquired.[56, 57] For the synthesis of $CoFe_2O_4/MnFe_2O_4$ core/shell NPs, preformed $CoFe_2O_4$ NPs dispersed in hexane were injected to the mixture of $MnCl_2$, $Fe(acac)_3$, oleic acid, oleylamine and trioctylamine. The reaction was then held at 365°C for 1 h and $MnFe_2O_4$ was overgrown onto the surface of the $CoFe_2O_4$ seeds to form a core/shell structure. As seen in Fig. 3, the resulted NPs are highly homogeneous in size, and electron energy-loss spectrum mapping analysis can confirm the formation of core/shell structure. If $MnFe_2O_4$ or Fe_3O_4 NPs were used as seeds, $CoFe_2O_4$ can be switched from the core to the shell based on the decomposition of $MnCl_2$ and $Fe(acac)_3$ under similar reaction conditions. Such a seed-mediated growth method has been successfully applied to generate $CoFe_2O_4$-based exchange-coupled nanosystems with different sizes, shapes and compositions. Song et al. synthesized $CoFe_2O_4/MnFe_2O_4$ and $MnFe_2O_4/CoFe_2O_4$ core/shell NPs with a core diameter of 6 nm, and the shell thickness could be precisely controlled from 0.5 to 3 nm.[37] Noh et al. reported the synthesis of cubic NPs, which are comprised of $Zn_{0.4}Fe_{2.6}O_4$ core (50 nm in edge) and $CoFe_2O_4$ shell (5 nm in thickness).[56]

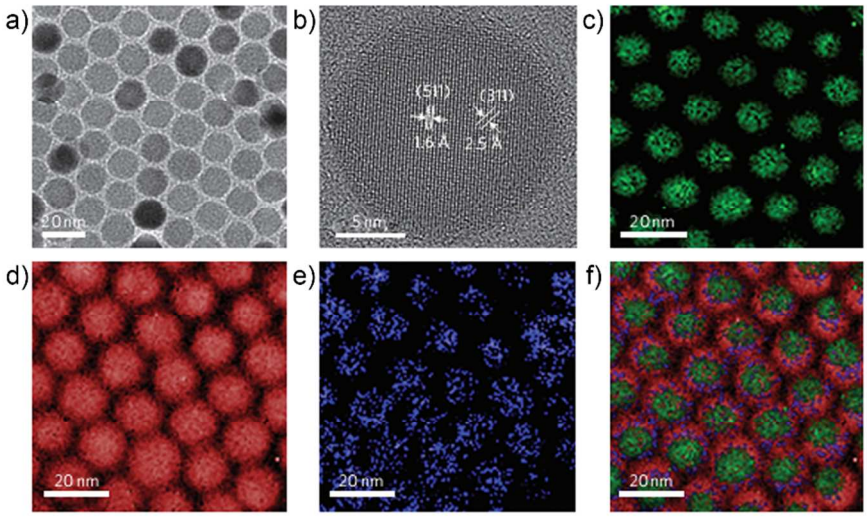

Fig. 3. a) TEM image and b) high-resolution TEM (HRTEM) image of 15nm $CoFe_2O_4/MnFe_2O_4$ core/shell NPs. c)-f) electron energy-loss spectrum mapped images. c) Co mapped image, d) Fe mapped image e), Mn mapped image and f) overlay image of c)-e). Reproduced with permission from Ref. 57. Copyright 2011 Nature Publishing Group.

Exchange coupling was also realized by utilizing self-assembly of appropriate magnetic NPs.[58, 59] For example, using $CoFe_2O_4$ and Fe_3O_4 NPs as building blocks, the binary superlattices were self-assembled by the liquid-air interfacial assembly approach, whereby a hexane solution of mixed $CoFe_2O_4$ and Fe_3O_4 NPs with appropriate concentration ratios was drop cast onto the diethylene glycol surface.[57] Continuous superlattices isostructural with $NaZn_{13}$ and $MgZn_2$ were formed by choosing NPs with different sizes. Removing the organic capping ligands present at the NP surface upon thermal annealing under vacuum at 400°C, exchange coupling between $CoFe_2O_4$ and Fe_3O_4 NPs could be introduced while the superlattices still maintained the periodic structure. More interestingly, by annealing the binary superlattices of self-assembled Fe_3O_4 and Co NPs, superlattice of $Fe_3O_4/CoFe_2O_4$ core/shell NPs was formed, leading to the dramatically increased coercivity.[58] During the thermally driven process, Co atoms from Co NPs first diffused into Fe_3O_4 matrix, and then the Fe^{2+} cations were replaced by these Co atoms through redox chemical reaction, giving a $CoFe_2O_4$ shell on the Fe_3O_4 surface.

FePt- and FePd-based nanocomposites

FePt and FePd alloys with the face-centered tetragonal (*fct*) structure (also known as $L1_0$ phase) are suitable candidates as hard magnetic materials owing to their large *K* and superior chemical stability.[60] In the structure, atomic layers of Fe and Pt (or Pd) stack alternatively along the [001] direction (the c-axis), which is the magnetic easy axis. For $L1_0$-FePt, the *K* value can reach as high as 6.6×10^6 J m^{-3}, which is due to the large spin-orbit coupling of the Pt site and the hybridization between Fe 3d and Pt 5d states. Note the FePt or FePd can also form a stable *fcc* structure, where the Fe and Pt (or Pd) atoms distribute randomly. These *fcc*-structured alloys are chemically disordered, and have much smaller anisotropy compared to the *fct*-structured counterparts.

Sun et al. developed a chemical strategy to synthesize monodisperse FePt NPs via thermal decomposition of iron pentacarbonyl, $Fe(CO)_5$ and reduction of $Pt(acac)_2$ in the presence of oleic acid and oleylamine as surfactants and 1,2-alkanediol as a mild reducing agent.[15] The $Fe(CO)_5/Pt(acac)_2$ ratio is found to be crucial for controlling the composition of the FePt NPs. The size of the FePt NPs can be finely tuned either by controlling the surfactant to metal ratio or by a seed-mediated growth method. Removing the additional reducing agent such as 1,2-alkanediol in the reaction, better size control

of the FePt NPs can be achieved.[61, 62] By varying the reaction conditions, FePt octapods, cuboctahedrons, truncated cubes, nanocubes, nanorods and nanowires were successfully prepared.[61-64] In spite of success in controlled synthesis of FePt NPs, the resulted FePt NPs are usually chemically disordered, which are not expected to have a large *K*. In order to obtain chemically ordered FePt, thermal annealing is necessary. By coating FePt NPs with MgO (or SiO_2), or dispersing them in NaCl matrix before annealing, sintering of FePt NPs can be prevented, making it possible to obtain dispersible $L1_0$-FePt NPs.[65-69]

To fabricate FePt-based exchange-coupled nanocomposites, Zeng et al. combined the chemical synthesis and self-assembly of NPs with subsequent thermal annealing process.[70] In the synthetic approach, FePt and Fe_3O_4 NPs with selected concentration, volume and sizes were mixed in hexane and used as building blocks. The three-dimensional binary assemblies were formed by solvent evaporation of the mixed NP dispersions. Fe_3O_4 and FePt NPs with different sizes and fixed mass ratio of 1:10 led to distinct assembly structures, as shown in Fig. 4. Fe_3O_4 and FePt NPs with both sizes of 4 nm gave a hexagonal lattice with random occupation of the two kinds of NPs (Fig. 4a), whereas phase segregation tended to appear when the size difference of NPs became larger (Fig. 4b-c). Annealing under a flow of Ar containing 5% H_2 at 650°C was applied to induce the phase transition from disordered FePt to ordered tetragonal FePt, resulting in the formation of FePt-Fe_3Pt hard-soft nanocomposites. When the binary assemblies containing FePt and Fe_3O_4 NPs of similar sizes (about 4 nm) were subject to annealing, the Fe_3Pt phase in the resulted sample was uniformly dispersed into the FePt matrix, and the Fe_3Pt phase dimension was below 10 nm. In contrast, for the binary assemblies contained Fe_3O_4 (12 nm) and $Fe_{58}Pt_{42}$ (4 nm) NPs, annealing process led to large α-Fe particles over 20 nm in diameter. Alternatively, a more convenient strategy was developed to control the dimension of different phases by using core/shell structured FePt/Fe_3O_4 NPs as building blocks.[71] Based on the seed-mediated growth process, FePt/Fe_3O_4 core/shell NPs were synthesized by the decomposition of $Fe(acac)_3$ in the mixture of 1,2-hexadecanediol, oleic acid, oleylamine and phenyl ether in the presence of FePt seeds (Fig. 4d). The thickness of Fe_3O_4 shell could be readily tuned from 0.5 to 3 nm by controlling the $Fe(acac)_3$/FePt ratio. The synthetic approach could be extended to produce FePt/$CoFe_2O_4$ core/shell NPs by adding $Co(acac)_2$ into the reaction.[36] When cubic FePt NPs were used as seeds, the Fe_3O_4 (or $CoFe_2O_4$) phase preferentially grew on a few selected facets, giving the bricklike shape.[72, 73] Owing to the unique topology, the thickness of both components can be tuned to a large extent, making it easy to control the ratio of soft-hard phases. However, forming $L1_0$-FePt-based nanocomposites needs a high temperature, which may cause partial diffusion of soft phase elements such as Fe or Co into the $L1_0$-FePt matrix. In order to prevent such diffusion and get a distinct soft phase, high temperature annealing process needs to be removed. Liu et al. presented a general protocol to build exchange-coupled nanocomposites with hard magnetic *fct*-FePt as the core and soft magnetic Co (or Ni, Fe_2C) as the shell.[74] In a typical procedure, dispersible $L1_0$-FePt NPs were prepared from thermal annealing of the *fcc*-FePt/Fe_3O_4/MgO composites. MgO coating was very effective to prohibit the diffusion in *fct*-formation process, and could be removed by acid washing. The $L1_0$-FePt NPs stabilized with oleic acid and oleylamine were used as seeds for the growth of the soft magnetic phases. The resulted nanocomposites possessed the core/shell configuration, and the shell thickness could be readily controlled by tuning the molar ratio between the seed and the precursor. Fig. 5 shows the TEM and HRTEM images of the representative FePt/Co core/shell NPs. The high-angle annular dark-field scanning TEM (HAADF-STEM) image (Fig 5c) and element analysis (Fig. 5d) confirm the FePt/Co core/shell nanostructure.

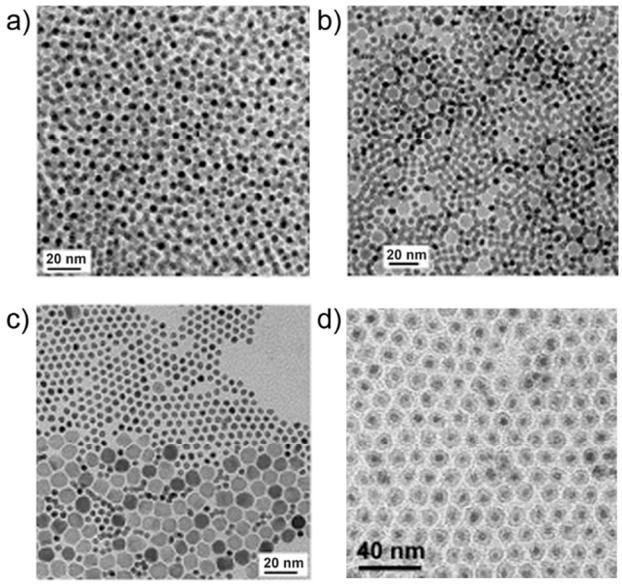

Fig. 4. a)-c) TEM images showing binary NP assemblies with a mass ratio of Fe_3O_4: FePt=1:10. a) Fe_3O_4 (4 nm):$Fe_{58}Pt_{42}$ (4 nm) assembly, b) Fe_3O_4 (8 nm): $Fe_{58}Pt_{42}$ (4 nm) assembly, and c) Fe_3O_4 (12 nm): $Fe_{58}Pt_{42}$ (4 nm) assembly. Reproduced with permission from Ref. 70. Copyright 2002 Nature Publishing Group. d) TEM image of core/shell FePt/Fe_3O_4 NPs with core/shell being 4 nm/0.5 nm. Reproduced with permission from Ref. 71. Copyright 2004 American Chemical Society.

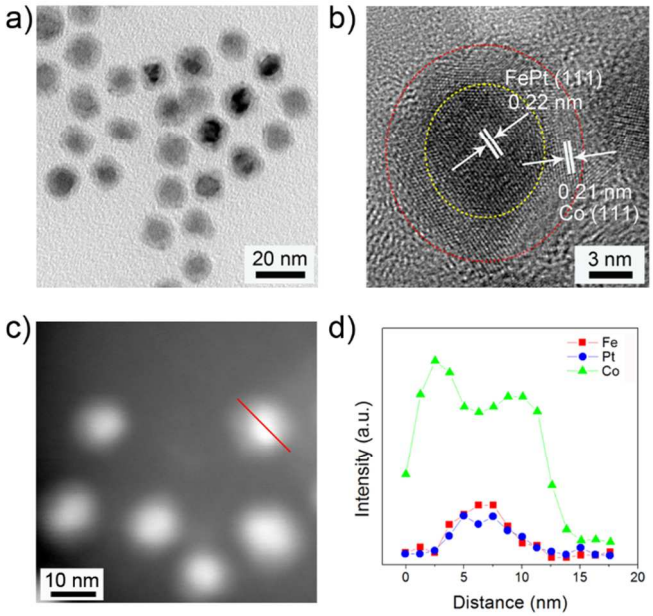

Fig. 5. a) TEM and b) HRTEM images of FePt/Co core/shell NPs. c) HAADF-STEM image of the FePt/Co NPs, and d) EDS profile obtained by scanning a single FePt/Co NP illustrated in

c). Reproduced with permission from Ref. 74. Copyright 2014 Wiley-VCH.

Similar to FePt, FePd with $L1_0$ structure also exhibits a large value of K (1.0×10^6 J m^{-3}). Although annealing process is still necessary to obtain $L1_0$-FePd-based nanocomposites, distinct Fe phase can exist along with $L1_0$-FePd phase by analyzing the FePd alloy equilibrium phase diagram. Therefore, the $L1_0$-FePd-Fe system is suitable for understanding exchange coupling between the magnetic phases. There are a few attempts via chemical method to fabricate $L1_0$-FePd-Fe nanocomposites. Teranishi et al. prepared $L1_0$-FePd-Fe nanocomposites by interfacial atom diffusion of anisotropically phase-segregated Pd/Fe_2O_3 NPs.[75] By mixing the heterostructured NPs with extra Pd NPs, the volume fraction of hard ($L1_0$-FePd)/soft (α-Fe) phases in the annealed sample could be controlled.[47] The O_3 treatment was applied to remove the organic capping agents before annealing, suppressing the formation of iron carbide that generally derived from the carbonization of α-Fe. The annealing temperature should be below 550 °C to prevent the formation of the disordered *fcc*-FePd phase. Alternatively, Yu et al. reported the preparation of $L1_0$-FePd-Fe nanocomposites converted from the urchin-like FePd-Fe_3O_4 composites via annealing.[76] During the process of the one-pot synthesis of urchin-like FePd-Fe_3O_4 composites (Fig. 6a-b), FePd NPs were formed at first by decomposition of $Fe(CO)_5$ and reduction of $Pd(acac)_2$ and were self-aggregation into FePd superparticles. At elevated reaction temperature, Fe_3O_4 started to nucleate and grow on FePd surface, resulting in a rod-like morphology. The urchin-like FePd-Fe_3O_4 composites were then annealed in a reducing atmosphere at appropriate temperature, giving $L1_0$-FePd-Fe nanocomposites as indicated by HRTEM image (Fig 6c) and elemental mappings of Pd and Fe (Fig. 6d-f).

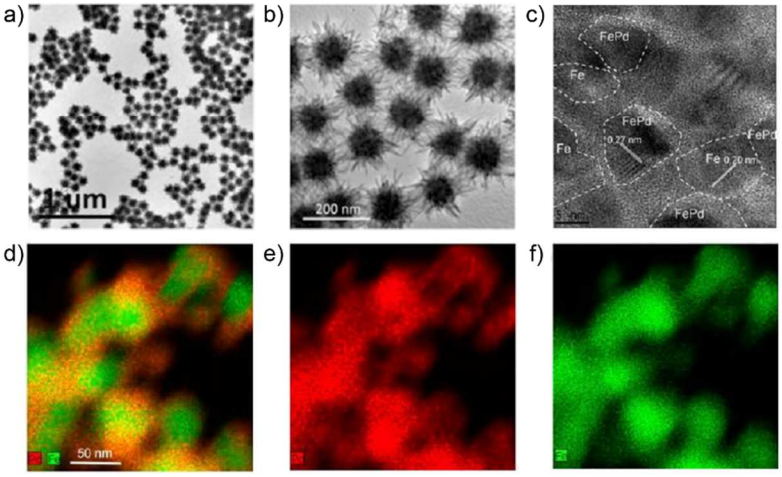

Fig. 6. a) and b) TEM images of the urchin-like FePd-Fe_3O_4 composites. c) HRTEM image of the $L1_0$-FePd-Fe nanocomposites with nanocrystalline grains of either $L1_0$-FePd or Fe indicated. d) Elemental mappings of Pd (red)/Fe (green) signals combined and single element e) Pd (red) and f) Fe (green). Reproduced with permission from Ref. 76. Copyright 2013 American Chemical Society.

RE-based nanocomposites

The RE intermetallics such as $SmCo_5$ and $Nd_2Fe_{14}B$ compounds have been the most important hard magnetic materials in modern society due to their superior intrinsic magnetic properties and relatively low cost per energy-density unit. $SmCo_5$ adopts a hexagonal $CaCu_5$-type crystal structure with Co and Co/Sm present in alternating layers along the c-axis. $SmCo_5$ exhibits a very large K value ($1.1\text{-}2.0\times10^7$ J m^{-3}) as well as a very high Curie temperature, which makes it suitable for high-temperature applications. The structure of $Nd_2Fe_{14}B$ compound is even more complex. Nd-Fe-B compound with the 2-14-1 stoichiometry has a tetragonal crystal structure containing 68 atoms per unit cell, in which magnetic moments of Fe and Nd atoms are parallel to the c-axis. Although anisotropy of $Nd_2Fe_{14}B$ is lower (~4×10^7 J m^{-3}) than that of $SmCo_5$, the magnetization is much higher due to the large content of iron in the compound.

Inspired by the success in the synthesis of cobalt ferrite, FePt and FePd NPs, researchers have tried chemical routes to prepare Sm-Co and Nd-Fe-B compounds. In the early attempts, solution phase approaches have been applied to synthesize the NPs by modulating the reaction conditions, the nature of the precursors, solvents, and capping agents, but the magnetic performance of the obtained compounds was much lower than that of the bulk counterparts.[2] The difficulty of synthesizing high-performance RE intermetallics lies on the electronegativity and instability of RE metals under ambient conditions. Recently, researchers found that a high temperature reductive annealing with Ca as reducing agent was very effective to get magnetic compounds with high purity and crystallization. Hou et al. reported a facile synthesis of $SmCo_5$ by a solution phase route combined with solid-state high-temperature reductive annealing.[77] Initially, core/shell-structured Co/Sm_2O_3 NPs were prepared by the decomposition of $Sm(acac)_3$ over the surface of the Co NPs. Subsequently, the Co/Sm_2O_3 core/shell NPs were subject to reductive annealing under Ar+5% H_2 at a temperature of 900 °C in the presence of metallic Ca. KCl as an inorganic solvent was used in the solid-state reaction for promoting interface diffusion between Sm and Co. Interestingly, by adjusting the $Sm(acac)_3$/Co ratio in the growth stage, core/shell NPs with a thicker Sm_2O_3 coating could be synthesized, leading to the formation of Sm_2Co_{17} under similar annealing condition. To prepare $SmCo_5$ and Sm_2Co_{17} NPs, Zhang et al. proposed a multi-step strategy by coating CaO on the Sm-Co-oxide NPs to prevent NPs from sintering at high temperature.[78] Washing off the CaO by water could leave dispersible Sm-Co NPs. Chemical synthesis of Nd-Fe-B compound is more difficult than Sm-Co due to the fact

that it consists of three elements rather than two. Among the reported approaches, sol-gel process followed by reduction annealing was effective.[79, 80] Deheri et al. prepared $Nd_2Fe_{14}B$ NPs with the size of ~65 nm by reductive annealing the mixed Nd-Fe-O oxides in the presence of CaH_2.[79] The oxides were derived from the annealed Nd-Fe-B gel, which was prepared using $NdCl_3 \cdot 6H_2O$, $FeCl_3 \cdot 6H_2O$, H_3BO_3, citric acid, and ethylene glycol. The reduction-diffusion was then held at 800 °C in vacuum, yielding desired $Nd_2Fe_{14}B$ phase with $Nd_2Fe_{14}BH_{4.7}$ and Fe as byproducts.

Involving the precursors containing Fe and/or Co in the synthesis of Sm-Co and Nd-Fe-B compounds can achieve exchange-coupled nanocomposites. In a typical synthesis of $SmCo_5$/Fe nanocomposites, Hou et al. mixed Fe_3O_4 NPs with SmCo-hydroxide, followed by annealing the mixture at high temperature in the presence of a strong reducing agent Ca and a dispersion medium KCl.[43] Preformed Fe_3O_4 NPs were embedded into Sm-Co-hydroxide matrix, and the molar ratio of Sm/Co/Fe was controlled by the mass ratio of the precursors. Analyzing the structures by X-ray diffraction (XRD) and TEM techniques, the nanocomposites consist of a hexagonal structured $SmCo_5$ and metallic Fe with the average grain sizes of 29 nm and 8 nm, respectively. In a similar process based on the precursors of NPs, Chaubey et al. reported a simple method to prepare $SmCo_5$/Fe nanocomposites by high temperature reduction of a NP mixture comprising of Sm_2O_3, Co and Fe, which was synthesized by thermal decomposition of metal precursors in the high-boiling-point solvent.[81] The concentration of Fe could be controlled by varying the initial molar ratio of $Fe(acac)_3$ in the reaction. Very recently, Yang et al. proposed a bottom-up method to chemically synthesize exchange-coupled single domain $SmCo_5$/Co core/shell nanocomposites by reductive annealing of $Sm[Co(CN)_6] \cdot 4H_2O$/graphene oxide particles.[82] In the synthesis, graphene oxide sheets which wrap on the surface of the $Sm[Co(CN)_6] \cdot 4H_2O$ crystals, were essential to restrain the growth of the crystal and control the size of the resulted $SmCo_5$/Co core/shell nanocomposites upon reductive annealing. In addition, graphene oxide sheets helped to sustain the $SmCo_5$ phase as single crystalline and facilitated the generation of Co shell on the surface of $SmCo_5$ phase. The formation of $SmCo_5$ and Co phases was confirmed by XRD analysis (Fig. 7a). The particles had an average size of 200 nm closed to single domain size of bulk $SmCo_5$ (Fig 7b-c), and were core-shell structures which consisted of single crystalline $SmCo_5$ as core, polycrystalline Co as shell and a coherent amorphous interlayer with thickness of 2 nm (Fig. 7d-f). Without GO wrapping, the $SmCo_5$ phase could also be obtained, but the products were aggregated with inhomogeneous size and shape, and adopted multi-domain structure. Interestingly, a series of Sm-Co-based exchange-coupled nanocomposites could be prepared by controlling the Co/Sm ratio in the starting materials. Increasing Co/Sm ratio from 3.5 to 3.7, the phase of Sm_2Co_{17} appears in the shell of the particles while the interior part still holds the component of single crystalline $SmCo_5$. Further increase of Co/Sm ratio would result in the formation of Sm_2Co_{17}/Co core/shell particles. In all types of the particles, the core of hard magnetic phase was single crystalline, which is beneficial to achieve large anisotropy of the exchange-coupled nanocomposites.

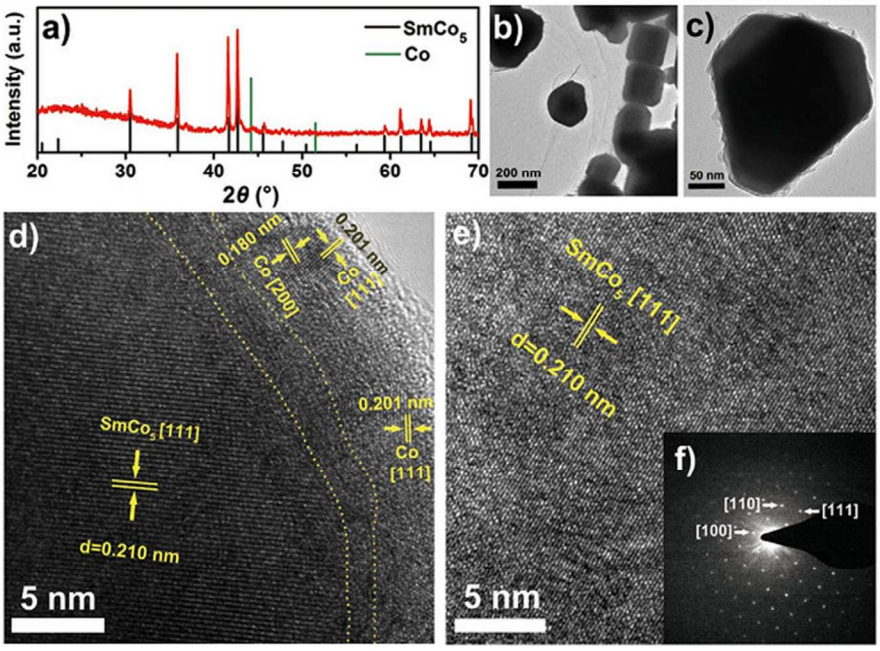

Fig. 7. a) XRD pattern and b) TEM image of $SmCo_5$/Co core/shell nanocomposites. c) TEM image of an isolated $SmCo_5$/Co core/shell particle. d) HRTEM image of the exterior part of $SmCo_5$/Co core/shell particle. e) HRTEM image of an arbitrary interior part of the particle. f) Selected area diffraction pattern of the $SmCo_5$/Co core/shell particle shown in c). Reproduced with permission from Ref. 82. Copyright 2013 Nature Publishing Group.

Applications of Exchange-coupled nanocomposites

Exchange-coupled nanocomposites as advanced permanent magnets

Permanent magnetic materials with the capability of maintaining a large magnetic flux in the absence of a

magnetizing field play a key role in human civilization and have been widely used in the construction of battery-driven tools, magnetic resonance imaging units, electric bicycles, electric-assisted vehicles, speakers, magnetic separation units, etc. The key figure of merit of permanent magnets can be assessed by the energy product, $(BH)_{max}$, which has been enhanced to ~56 MGOe by the development of Nd-Fe-B magnets during the past decades. High-energy product magnets are preferred because they enable the design and manufacture of smaller and lighter-weight devices that have great advantages for the improvement in energy efficiency. Large value of $(BH)_{max}$ requires the permanent magnet to have a M_s as high as possible and an appropriate H_c. Although numerous efforts have been done for seeking a new kind of permanent magnetic material after Nd-Fe-B magnets, no major breakthrough has been made in single compound or alloy. However, the discovery of exchange coupling effects offers a new approach for the development of high-energy product permanent magnets by making the best of the strengths of soft and hard magnetic phases. Skomski and Coey theoretically predicted that in an ideal exchange-coupled magnets consisting of anisotropic $Sm_2Fe_{17}N_3/Fe_{67}Co_{33}$, the value of $(BH)_{max}$ can be as high as 120 MGOe.[23]

As described in Section 2, the keys to obtain exchange-coupled nanocomposite magnets with high-energy density are mainly (1) magnetic properties of soft and hard magnetic phases, (2) volume fraction of hard/soft magnetic phases, (3) grain size and distribution of hard/soft magnetic phases, (4) interface between hard/soft magnetic phases and (5) alignment of the grains. The most impressive and unique advantage of chemical routes compared to other conventional methods is the well control of the hard and soft phases at the nanoscale for effective exchange coupling. Zeng et al. first produced exchange-coupled permanent magnets with considerably high energy product based on chemical synthesis.[70] FePt-Fe_3Pt nanocomposites made from the annealed $Fe_3O_4/Fe_{58}Pt_{42}$ assemblies with different particle sizes show distinct magnetic behavior. The hysteresis loop (Fig. 8a) of FePt-Fe_3Pt nanocomposites from Fe_3O_4 (4 nm):$Fe_{58}Pt_{42}$ (4 nm) assembly showing single-phase-like behavior indicates effective exchange coupling between FePt and Fe_3Pt, but loop (Fig. 8b) of nanocomposites from Fe_3O_4 (12 nm):$Fe_{58}Pt_{42}$ (4 nm) assembly shows a kink at low field. The dimension of the Fe_3Pt phase was controlled to be at about 5 nm, which is smaller than twice the domain wall width of the hard phase, ensuring effective exchange coupling for the enhancement of $(BH)_{max}$. In addition to the size effect, volume fraction of the soft phase, which could be readily tuned by the mass ratio of the starting materials, also contributed to the high value of $(BH)_{max}$. The isotropic FePt-Fe_3Pt nanocomposites derived from Fe_3O_4/FePt NP assembly have an energy product of 20.1 MGOe, which exceeds the theoretical limit of 13 MGOe for non-exchange-coupled isotropic FePt by over 50%. Extending the strategy to prepare other FePt-based nanocomposite magnets, high value of $(BH)_{max}$ exceeding the theoretical limit for non-exchange-coupled isotropic FePt was also accessible. Zeng et al. used FePt/Fe_3O_4 core/shell NPs as building blocks to form nanocomposites, and the optimal value of $(BH)_{max}$ tuned by the Fe_3O_4 thickness could be as high as 18 MGOe.[71] FePt/FeCo exchange-coupled nanocomposites obtained from 8 nm/8 nm FePt/$CoFe_2O_4$ by thermal annealing gave an energy product of 15.5 MGOe.[72] These early studies not only proved the effects of exchange coupling on the enhancement of the energy product but also showed great potential for making three-dimensional magnets with high energy product by a bottom-up approach.[83] In order to form high-density bulk materials based on the NP building blocks, compaction techniques like warm compaction which is performed at modest temperatures and under certain pressures have been developed.[84-86] The powders consisting of FePt and Fe_3O_4 NPs were compacted with a warm-compaction press under pressure of 2.5 and 3.8 GPa for 10 min at different temperature, giving bulk samples with dimensions of Φ6 mm×1.5 mm and Φ3 mm×1.2 mm, respectively.[84] High temperature and high pressure were beneficial to achieve satisfactory density of the bulk samples and were helpful to facilitate the formation of $L1_0$-FePt phase. Moreover, the temperature strongly impacted the magnetic property of the products. The temperature of above 400 °C was essential to derive high H_c since $L1_0$-FePt phase with high K was formed. On the other hand, higher temperature could lead to higher density of the samples with a reduced surface effect, thus resulting in increased M_s. By optimizing the parameters of warm-compaction press, the value of $(BH)_{max}$ could be up to about 15.5 MGOe, and could be further improved to 16.3 MGOe by a post-annealing at 550 °C under forming gas (93%Ar + 7%H_2) for 1 h.

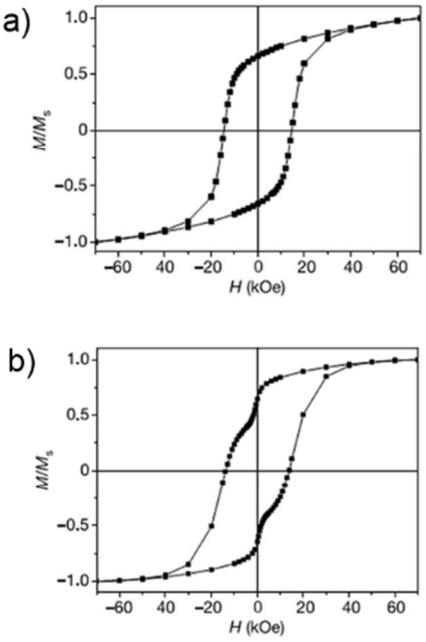

Fig. 8. Typical hysteresis loops of FePt-Fe_3Pt nanocomposites made from the annealed a) Fe_3O_4 (4 nm):$Fe_{58}Pt_{42}$ (4 nm) assembly and b) Fe_3O_4 (12 nm):$Fe_{58}Pt_{42}$ (4 nm) assembly with particle mass ratio being kept constantly at Fe_3O_4:FePt=1:10. Reproduced with permission from Ref. 70. Copyright 2002 Nature Publishing Group.

In the case of FePd-Fe nanocomposites, significant advance has been made to obtain large $(BH)_{max}$. A comprehensive study by Sakuma et al. showed the effects of annealing temperature and the hard/soft phase volume fraction on the exchange coupling and magnetic properties of the nanocomposites.[47] The mixture of Pd/γ-Fe_2O_3 heterostructured NPs and pure Pd NPs annealed from 450 to 550 °C was used to test the magnetization curves. For the samples annealed below 525 °C, the magnetization curves behaved like a single magnetic phase without unusual drops or kinks, suggesting effective exchange interaction between FePd and Fe phases. In contrast, the sample

annealed at 550 °C had a hysteresis loop that is constricted, indicating that the soft phase was no longer coupled with the hard phase. In order to obtain high H_c, the optimal annealing temperature should lie between 475 and 500 °C by considering the formation of highly ordered $L1_0$-FePd and the avoidance of the phase-segregation and the coalescence of α-Fe. To clarify the effect of the hard/soft phase volume fraction on the magnetic properties, samples with the FePd/Fe volume ratio of 44/56, 82/18, and 100/0 were investigated. High fraction of Fe resulted in increased M_s and M_r, but deteriorated the H_c. Combing the consideration of the effects of annealing temperature and the hard/soft phase volume fraction, the value of $(BH)_{max}$ could be optimized to 10.3 MGOe in the nanocomposites formed by annealing at 500 °C with the FePd/Fe volume ratio of 82/18. Such a value is considerably high for nanocomposites without using platinum or RE elements.

The magnetic properties of RE-based magnets prepared by chemical methods have been improved significantly in the past decade. In the early stage, researchers tried solution synthetic strategy to directly obtain the products, however, H_c of resulted magnets was much lower than what was expected. The main reason for the low H_c is the phase purity and crystallinity of the hard phase. A big improvement in H_c of Sm-Co-based magnets was made by utilizing the annealing process with Ca. Hou et al. reported the preparation of $SmCo_5$ magnets exhibiting a H_c of 8 kOe at room temperature.[77] By a similar reduction process from Sm-Co-oxide NPs, Zhang et al. acquired sintered $SmCo_5$ with a large H_c of 20.5 kOe at room temperature.[78] These studies indicated that high temperature reduction was helpful for the formation of highly crystalline Sm-Co phase with superior magnetic properties. For the Sm-Co-based nanocomposites, such a reduction process was also critical. In order to control both the coercivity and magnetization of the $SmCo_5$/Fe nanocomposite magnets, Hou et al. exploited reductive annealing of the mixture of Sm-Co-O and Fe_3O_4 NP and varied the Fe fraction (from 0 to 2.9) in the nanocomposites.[43] By analyzing the magnetization curves at room temperature, it was found that the $SmCo_5/Fe_{1.5}$ shows a H_c of 6.05 kOe (8.8 kOe for $SmCo_5$) and an enhanced M_r at 56 emu/g (45 emu/g for $SmCo_5$), and the $SmCo_5/Fe_{0.23}$ have the largest coercivity at 11.6 kOe. Alternatively, Chaubey et al. also demonstrated the effect of doping percentage of Fe on the magnetic properties for $SmCo_5$/Fe nanocomposites.[81] With increasing Fe fraction in the nanocomposites, the coercivity decreases whereas magnetization increases. As a result, $SmCo_{6.5}Fe_{1.2}$ exhibited a largest $(BH)_{max}$ of 7.8 MGOe compared to $SmCo_5$ and $SmCo_{5.5}Fe_{0.6}$ nanocomposites. Considering the size effect on the magnetism, it is possible to further improve the magnetic performance by controlling the grain size of Sm-Co phase close to the critical single domain size. Sm-Co phase with relatively small grain size is not preferred due to the fact that it not only holds diminished ferromagnetic properties but also endures easily oxidation. For example, 6 nm $SmCo_5$ NPs only possessed coercivity of 7.2 kOe,[78] while for the single domain $SmCo_5$ particles with average size of about 300 nm, the coercivity can reach up to 23.7 kOe.[87] However, it is still very challenging to achieve Sm-Co phase with single domain state for the Sm-Co-based nanocomposites. Yang et al. recently synthesized exchange-coupled single domain $SmCo_5$/Co magnets with a core/shell structure and an average size of 200 nm, giving a large H_c of 20.7 kOe, M_s of 82 emu g^{-1} and $(BH)_{max}$ of 10 MGOe (Fig. 9a).[82] For comparison, multi-domain $SmCo_5$ magnets synthesized by a similar approach had irregular shapes as well as random sizes ranging from 100 nm to 600 nm, and they presented deteriorative $(BH)_{max}$ of 3 MGOe with H_c of 13.7 kOe and M_s of 58 emu g^{-1}. More interestingly, $SmCo_5/Sm_2Co_{17}$ magnets produced by increasing Co/Sm ratio in the starting materials still maintained a single domain core of $SmCo_5$, ensuring a large coercivity for the magnets. With the increase of Sm_2Co_{17} amount in the magnets, the H_c of magnets decreases from 20.7 kOe to 7.1 kOe while the M_s increased from 82 to 114 emu g^{-1}, and $SmCo_5$/40%Sm_2Co_{17} had the largest $(BH)_{max}$ of 8 MGOe (Fig. 9b-c).

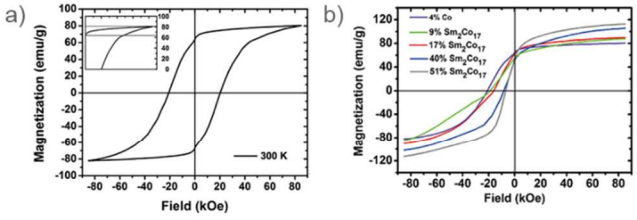

c)

$SmCo_5$ with	4% Co	9% Sm_2Co_{17}	17% Sm_2Co_{17}	40% Sm_2Co_{17}	51% Sm_2Co_{17}
Hc (kOe)	20.7	19.1	16.1	8.5	7.1
Ms (emu/g)	82	85	90	102	114
Mr (emu/g)	62.46	55.83	61.06	53.51	55.37
$(BH)_{max}$ (MG·Oe)	10	6.5	8	4.5	4.4

Fig. 9. a) Room temperature hysteresis loop of $SmCo_5$/Co magnets. b) Room temperature hysteresis loops and c) magnetic properties of $SmCo_5$-based nanocomposites with various compositions. Reproduced with permission from Ref. 82. Copyright 2013 Nature Publishing Group.

Exchange-coupled nanocomposites as mediators for therapeutics

Due to the capability of generating heat in the external alternating current (a.c.) magnetic field, magnetic NPs have attracted considerable attention as one of the promising candidates for disease therapy.[88-91] Thermal energy is produced by the magnetic mediators through different processes of magnetic losses (Fig. 10a), including Néel and Brownian spin relaxations, and hysteresis loss.[92, 93] The specific loss power (SLP) which is measured in watts per gram of magnetic materials is used to describe the therapeutic capability of the magnetic materials. A large value of SLP is highly desired for enhancing energy transfer efficiency and reducing the amount of the magnetic mediators in the cancer treatment. According to the different types of energy dissipation, the SLP value can be optimized by tailoring the properties of the magnetic materials. For the superparamagnetic NPs, SLP primarily depends on Néel and Brownian spin relaxations, so the volume, M_s, and K of the NPs are essential (Fig. 10b).[94-97] It is found theoretically and experimentally that NPs with a certain particle size and K can lead to a maximum SLP value. Using ferrite magnetic NPs as an example, it is calculated that the K between 0.5×10^4 and 4.0×10^4 J m^{-3}, and size between 10 and 30 nm can give high SLP values from 1,000 to 4,000 W g^{-1}.[57] In addition, high M_s and monodispersity are also beneficial to increase SLP. For the ferro- and ferrimagnetic NPs, the amount of dissipated heat is proportional to the area of the hysteresis loop, and hence to the frequency of the alternating magnetic field.[93] It is worth noting that the SLP value attributed to hysteresis loss is much larger than that originates from spin relaxations (Fig. 10c), and therefore, ferromagnetic NPs with optimized H_c and M_s are

ideal for effective hyperthermia. Schematics of the experimental apparatus and in vivo hyperthermia treatment in a mouse are shown in Fig. 10d,e.

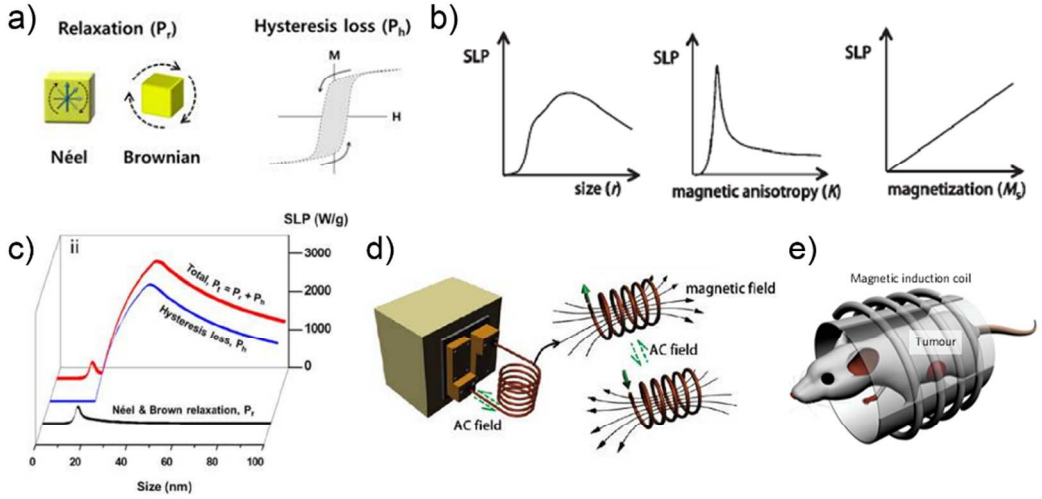

Fig. 10. Magnetic mediators for hyperthermia. a) Schematic representation of the major mechanisms for heat dissipation. b) The plot of SLP based on size, K and M_s. c) Size dependent SLP resulted from relaxation loss and hysteresis loss. d) Experimental apparatus. e) Schematics of in vivo hyperthermia treatment in a mouse. Reproduced with permission from Ref. 18, 56, 57. Copyright 2012, 2011 American Chemical Society. Copyright 2011 Nature Publishing Group.

As mentioned above, maximum SLP value is related to the appropriate size, size distribution, K, H_c and M_s of the NPs. One can achieve these requirements as desired by rationally engineering the magnetic materials. Owing to the large magnetization, candidates like Fe, FeCo and zinc-doped metal ferrites exhibit high heating efficiency for the thermal treatment of cancer and other diseases.[98-100] $(Zn_{0.4}Mn_{0.6})Fe_2O_4$ NPs with a large M_s value of 175 emu g^{-1} and high monodispersity (size distribution < 5%) have the SLP value of 432 W g^{-1} when the frequency and amplitude of the applied magnetic field are 500 kHz and 37 kA m^{-1}, respectively.[98] The Fe_3O_4 coated Fe NPs with a drastically increased stability and magnetic moment (M_s = 164 emu g^{-1}) were demonstrated to exhibit high heating efficiency in the field fulfilling the physiological limitations.[99] Besides, maghemite (γ-Fe_2O_3) with an appropriate K of 1.6×10^4 J m^{-3} also possess high thermal energy transfer capability.[94]

Exchange coupling between soft/hard magnetic phases allows optimal tuning of K and M_s values in particular, making it possible to achieve high SLP value. $CoFe_2O_4$-based NPs with a core/shell structure have been used to examine the tunability of K and the magnetic heating power. As described in Section 2.1, the synthesis of well controlled $CoFe_2O_4$-based nanocomposites can be realized by a seed-mediated growth method. By varying the combination of the core and shell components in the magnetically coupled binary system, core/shell structured $CoFe_2O_4/MnFe_2O_4$, $CoFe_2O_4/Fe_3O_4$, $MnFe_2O_4/CoFe_2O_4$ and $Fe_3O_4/CoFe_2O_4$ NPs were prepared, giving the K values in the optimal range (~0.5×10^4 to 4.0×10^4 J m^{-3}) for high SLP values.[57] Surprisingly, the SLPs of these core/shell NPs exhibit values from 1,000 to 4,000 W g^{-1} under an a.c. magnetic field of 500 kHz at 37.3 kA m^{-1}, which are approximately one order of magnitude higher than that of single-component NPs (from 100 to 450 W g^{-1}), suggesting the positive effect of the exchange coupling. Moreover, by extending the exchange coupled binary system to the magnetic phases with high M_s, researchers obtained $Zn_{0.4}Co_{0.6}Fe_2O_4/Zn_{0.4}Mn_{0.6}Fe_2O_4$ core/shell NPs with unprecedentedly high SLP value of 3,886 W g^{-1}, which is 1.7 times higher than that for $CoFe_2O_4/MnFe_2O_4$ core/shell NPs and 34 times larger than that for commercial iron oxide NPs. Such exchange-coupled NPs were demonstrated to have high efficacy for hyperthermia in cancer cell studies. For example, $CoFe_2O_4/MnFe_2O_4$ core/shell NPs dispersed in normal saline were directly injected into the tumor of the nude mice xenografted with cancer cells (U87MG). Then the mouse received hyperthermia treatment for 10 min under an a.c. magnetic field of 500 kHz at 37.3 kA m^{-1}. It was found that the tumor was eliminated by day 18 after treatment by measuring the tumor volume (Fig. 11a, b). Immunofluorescence histological image of the tumor region after hyperthermia treatment showing the absence of fluorescence could also indicate the elimination of tumor (Fig. 11c). For comparison, when commercial iron oxide NPs or the chemotherapeutic drug doxorubicin with the same dosage of $CoFe_2O_4/MnFe_2O_4$ NPs were used to treat the mice, the tumors could not be eliminated in one month. In addition to the $CoFe_2O_4$-based nanocomposites, Meffre et al. coated iron carbide on the iron NPs to tune the K value. The shell of iron carbide was used to reduce the K value while keeping high M_s, resulting in a substantially increase of SLP value in moderate fields.[101]

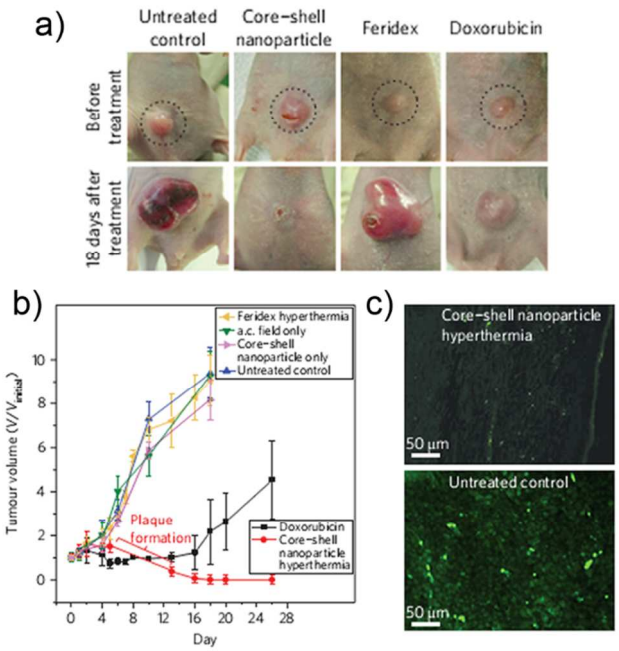

Fig. 11. a) Nude mice xenografted with cancer cells (U87MG) before treatment and 18 days after treatment with untreated control, $CoFe_2O_4/MnFe_2O_4$ hyperthermia, Feridex hyperthermia and doxorubicin, respectively. b) Plot of tumour volume versus days after treatment with $CoFe_2O_4/MnFe_2O_4$ core/shell NP hyperthermia, doxorubicin, Feridex hyperthermia, a.c. field only, core/shell NPs only and untreated control. c) Immunofluorescence histological images of the tumour region after hyperthermia treatment with $CoFe_2O_4/MnFe_2O_4$ core/shell NPs and the control tumour region. Reproduced with permission from Ref. 57. Copyright 2011 Nature Publishing Group.

In order to further enhance the energy transfer efficiency of the NP mediators, ferro- and/or ferrimagnetic NPs have been considered due to the fact that they can produce large thermal energy by hysteresis loss. Using the concept of exchange coupling, researchers are also able to tune the magnetism of ferro- and/or ferrimagnetic NPs with respect to properties such as M_s, K, and H_c. A comprehensive study by Noh et al. showed the effect of exchange coupling in cubic shaped $Zn_{0.4}Fe_{2.6}O_4/CoFe_2O_4$ core/shell NPs on controlling the magnetism and maximizing heat emission efficiency.[56] Taking advantage of cubic shape that contains less disordered spins compared to spherical shape, $Zn_{0.4}Fe_{2.6}O_4$ nanocubes with M_s tunable from 165 to 200 emu $g_{(Fe+Zn)}^{-1}$ by the size change were used as the soft magnetic phase to provide large M_s. However, the $Zn_{0.4}Fe_{2.6}O_4$ nanocubes possess very small H_c (less than 140 Oe) even though the size was tuned close to the critical single domain size. To attain increased H_c, hard magnetic phase of $CoFe_2O_4$ was grown on the surface of $Zn_{0.4}Fe_{2.6}O_4$ nanocubes by the seed-mediated growth method, and as a result, $Zn_{0.4}Fe_{2.6}O_4$ is strongly exchange-coupled with $CoFe_2O_4$. The resulted core/shell nanocubes exhibits significantly increased H_c of 1900 Oe while maintaining relatively high M_s of ~130 emu g^{-1}. At an alternative magnetic field of 500 kHz with 37.4 kA m^{-1}, the exchange-coupled nanocubes have extremely large SLP value of 10600 W g^{-1}, which is more than twice the value of uncoated $Zn_{0.4}Fe_{2.6}O_4$ nanocubes with optimized size. The core/shell nanocubes exhibit high efficacy for hyperthermia treatment of the colon cancer cell line, DLD-1, and its Doxorubicin resistant cell line, DLD-1-ADR. After the hyperthermia treatment for 3 min under the magnetic field of 500 kHz at 37.4 kA m^{-1}, the death of both drug resistant cells and normal cancer cells could be almost 100% with NP dosage of 200 μg mL^{-1}. At the same NP dosage, the cell death is only 84% for uncoated $Zn_{0.4}Fe_{2.6}O_4$ nanocubes. The disappearance of green fluorescence in fluorescent images of DLD-1-ADR cell lines also confirmed high efficacy of hyperthermia treatment by the core/shell nanocubes.

Summary and perspective

Chemical synthesis of exchange-coupled nanocomposites has made great achievements over the past decades. However, synthesis of exchange-coupled nanocomposites especially RE-based nanocomposites with desired magnetic performance is still very challenging. For example, impurities are often discovered in RE-based nanocomposites, and the size of the hard phase is difficult to control. Soft phases like Fe or FeCo with very small size, which is required for effective exchange coupling, are not stable in the air, thus the magnetization will significantly decrease. Although large enhancement of $(BH)_{max}$ is accessible for chemically synthesized FePt and Sm-Co-based nanocomposite magnets (~20 MGOe) compared to their single-phase counterparts, the value of $(BH)_{max}$ is much less than that of anisotropic $Nd_2Fe_{14}B$-based magnets. The success in the preparation of exchange-coupled FePt- and $Nd_2Fe_{14}B$-based films with extremely high $(BH)_{max}$ indicate that alignment of the easy anisotropy axes of the hard-phase grains is essential for the fabrication of superstrong permanent magnets. However, how to produce bulk nanostructured magnets with well-aligned and homogenously distributed grains is still a big problem that needs to be solved. As a result, it requires not only scale-up fabrication of the building blocks with well controlled size, phase and composition but also effective processing techniques. High-pressure warm compaction shows the potential to form high-density bulk materials with homogenous nanoscale morphology, but the techniques for making textured grains need to be developed. The aligning techniques that utilize an appropriate substrate or an external field in the thin film systems seem not suitable for nanostructured bulk magnets. Ways like severe plastic deformation and magnetic field assisted annealing are under investigation.

The development of exchange-coupled nanocomposites prepared by chemical synthesis is significant for magnetic hyperthermia and energy-related applications. High-energy product magnets are highly demanded for reducing the size and improving the energy efficiency of devices that utilize permanent magnets. The nanocomposites as mediators for heat induction are promising in cancer treatment. The deep understanding of exchange coupling and nanomagnetism will provide a guideline to produce magnetic mediators with enhanced energy transfer efficiency. The SLP values will be further increased based on the better control on the size, phase, interface and composition by chemical ways. More research is needed for the development of a variety of systems relying on heat induction such as thermal imaging and thermosensitive drug release. It is expected that exchange-coupled nanocomposites made from chemical synthesis will be widely applied in magnetic, biomedical and nanotechnology fields.

Acknowledgements

This work was supported by the National Basic Research Program of China (grant number 2010CB934601), the NSFC (grant numbers 51125001, 51172005, and 90922033), the Natural Science Foundation of Beijing (grant number 2122022), and the Doctoral Program (grant number 20120001110078).

Notes and references

[a] Department of Materials Science and Engineering, College of Engineering, Peking University, Beijing 100871, China. E-mail: hou@pku.edu.cn.

[b] College of Chemistry and Molecular Engineering, Peking University, Beijing 100871, China. E-mail: gaosong@pku.edu.cn.

1. O. Gutfleisch, M. A. Willard, E. Bruck, C. H. Chen, S. G. Sankar and J. P. Liu, *Adv. Mater.*, 2011, **23**, 821-842.
2. N. Poudyal and J. P. Liu, *J. Phys. D: Appl. Phys.*, 2013, **46**, 043001.
3. L. H. Lewis and F. Jimenez-Villacorta, *Metall. Mater. Trans. A-Phys. Metall. Mater. Sci.*, 2013, **44A**, 2-20.
4. C. Yang and Y. L. Hou, *Rare Metals*, 2013, **32**, 105-112.
5. J. M. D. Coey, *IEEE Trans. Magn.*, 2011, **47**, 4671-4681.
6. J. M. D. Coey, *Scripta Mater.*, 2012, **67**, 524-529.
7. R. Skomski, P. Manchanda, P. Kumar, B. Balamurugan, A. Kashyap and D. J. Sellmyer, *IEEE Trans. Magn.*, 2013, **49**, 3215-3220.
8. H. Zeng and S. Sun, *Adv. Funct. Mater.*, 2008, **18**, 391-400.
9. R. Hao, R. Xing, Z. Xu, Y. Hou, S. Gao and S. Sun, *Adv. Mater.*, 2010, **22**, 2729-2742.
10. U. Jeong, X. Teng, Y. Wang, H. Yang and Y. Xia, *Adv. Mater.*, 2007, **19**, 33-60.
11. A. H. Lu, E. L. Salabas and F. Schuth, *Angew. Chem. Int. Ed.*, 2007, **46**, 1222-1244.
12. N. A. Frey, S. Peng, K. Cheng and S. H. Sun, *Chem. Soc. Rev.*, 2009, **38**, 2532-2542.
13. D. L. Huber, *Small*, 2005, **1**, 482-501.
14. J. P. Wang, *Proc. IEEE*, 2008, **96**, 1847-1863.
15. S. Sun, C. B. Murray, D. Weller, L. Folks and A. Moser, *Science*, 2000, **287**, 1989-1992.
16. D. Ho, X. Sun and S. Sun, *Acc. Chem. Res.*, 2011, **44**, 875-882.
17. Y. W. Jun, J. W. Seo and J. Cheon, *Acc. Chem. Res.*, 2008, **41**, 179-189.
18. D. Yoo, J. H. Lee, T. H. Shin and J. Cheon, *Acc. Chem. Res.*, 2011, **44**, 863-874.
19. E. F. Kneller and R. Hawig, *IEEE Trans. Magn.*, 1991, **27**, 3588-3600.
20. R. Skomski and J. M. D. Coey, *IEEE Trans. Magn.*, 1994, **30**, 607-609.
21. T. Schrefl, H. Kronmüller and J. Fidler, *J. Magn. Magn. Mater.*, 1993, **127**, L273-L277.
22. R. Coehoorn, D. B. Demooij and C. Dewaard, *J. Magn. Magn. Mater.*, 1989, **80**, 101-104.
23. R. Skomski and J. M. D. Coey, *Phys. Rev. B*, 1993, **48**, 15812-15816.
24. R. Coehoorn and C. de Waard, *J. Magn. Magn. Mater.*, 1990, **83**, 228-230.
25. T. Leineweber and H. Kronmuller, *J. Magn. Magn. Mater.*, 1997, **176**, 145-154.
26. T. Nagahama, K. Mibu and T. Shinjo, *J. Phys. D: Appl. Phys.*, 1998, **31**, 43-49.
27. E. E. Fullerton, J. S. Jiang and S. D. Bader, *J. Magn. Magn. Mater.*, 1999, **200**, 392-404.
28. Z. J. Guo, J. S. Jiang, J. E. Pearson, S. D. Bader and J. P. Liu, *Appl. Phys. Lett.*, 2002, **81**, 2029-2031.
29. Z. S. Shan, J. P. Liu, V. M. Chakka, H. Zeng and J. S. Jiang, *IEEE Trans. Magn.*, 2002, **38**, 2907-2909.
30. G. Asti, M. Solzi, M. Ghidini and F. M. Neri, *Phys. Rev. B*, 2004, **69**, 174401.
31. A. J. Zambano, H. Oguchi, I. Takeuchi, Y. Choi, J. S. Jiang, J. P. Liu, S. E. Lofland, D. Josell and L. A. Bendersky, *Phys. Rev. B*, 2007, **75**, 144429.
32. J. P. Liu, E. Fullerton, O. Gutfleisch and D. J. Sellmyer, *Nanoscale Magnetic Materials and Applications*, Springer, Berlin, 2009.
33. J. S. Jiang, J. E. Pearson, Z. Y. Liu, B. Kabius, S. Trasobares, D. J. Miller, S. D. Bader, D. R. Lee, D. Haskel, G. Srajer and J. P. Liu, *Appl. Phys. Lett.*, 2004, **85**, 5293-5295.
34. R. Skomski, G. C. Hadjipanayis and D. J. Sellmyer, *J. Appl. Phys.*, 2009, **105**, 07A733.
35. S. Sato, S. J. Lee, C. Mitsumata, H. Yanagihara and E. Kita, *J. Appl. Phys.*, 2011, **109**, 083904.
36. H. Zeng, S. Sun, J. Li, Z. L. Wang and J. P. Liu, *Appl. Phys. Lett.*, 2004, **85**, 792-794.
37. Q. Song and Z. J. Zhang, *J. Am. Chem. Soc.*, 2012, **134**, 10182-10190.
38. E. C. Stoner and E. P. Wohlfarth, *Philos. Trans. R. Soc. A-Math. Phys. Eng. Sci.*, 1948, **240**, 599-642.
39. D. Goll, M. Seeger and H. Kronmuller, *J. Magn. Magn. Mater.*, 1998, **185**, 49-60.
40. E. P. Wohlfarth, *J. Appl. Phys.*, 1958, **29**, 595-595.
41. P. E. Kelly, K. Ogrady, P. I. Mayo and R. W. Chantrell, *IEEE Trans. Magn.*, 1989, **25**, 3880-3883.
42. R. W. Gao, W. C. Feng, W. Chen, B. Wang, G. B. Han and P. Zhang, *Chin. Sci. Bull.*, 2002, **47**, 1166-1169.
43. Y. Hou, S. Sun, C. Rong and J. P. Liu, *Appl. Phys. Lett.*, 2007, **91**, 153117-153113.
44. C. B. Rong, V. Nandwana, N. Poudyal, Y. Li, J. P. Liu, Y. Ding and Z. L. Wang, *J. Phys. D: Appl. Phys.*, 2007, **40**, 712-716.
45. K. Kang, L. H. Lewis, J. S. Jiang and S. D. Bader, *J. Appl. Phys.*, 2005, **98**, 113906.
46. C. L. Harland, L. H. Lewis, Z. Chen and B. M. Ma, *J. Magn. Magn. Mater.*, 2004, **271**, 53-62.
47. N. Sakuma, T. Ohshima, T. Shoji, Y. Suzuki, R. Sato, A. Wachi, A. Kato, Y. Kawai, A. Manabe and T. Teranishi, *Acs Nano*, 2011, **5**, 2806-2814.
48. J. E. Davies, O. Hellwig, E. E. Fullerton, J. S. Jiang, S. D. Bader, G. T. Zimanyi and K. Liu, *Appl. Phys. Lett.*, 2005, **86**, 262503.
49. G. Srajer, L. H. Lewis, S. D. Bader, A. J. Epstein, C. S. Fadley, E. E. Fullerton, A. Hoffmann, J. B. Kortright, K. M. Krishnan, S. A. Majetich, T. S. Rahman, C. A. Ross, M. B. Salamon, I. K. Schuller, T. C. Schulthess and J. Z. Sun, *J. Magn. Magn. Mater.*, 2006, **307**, 1-31.
50. I. Betancourt and H. A. Davies, *Mater. Sci. Technol.*, 2010, **26**, 5-19.
51. J. H. Lee, Y. M. Huh, Y. W. Jun, J. W. Seo, J. T. Jang, H. T. Song, S. Kim, E. J. Cho, H. G. Yoon, J. S. Suh and J. Cheon, *Nat. Med.*, 2007, **13**, 95-99.

52. Y. Yu, A. Mendoza-Garcia, B. Ning and S. Sun, *Adv. Mater.*, 2013, **25**, 3090-3094.
53. Q. Song and Z. J. Zhang, *J. Am. Chem. Soc.*, 2004, **126**, 6164-6168.
54. S. Sun and H. Zeng, *J. Am. Chem. Soc.*, 2002, **124**, 8204-8205.
55. S. Sun, H. Zeng, D. B. Robinson, S. Raoux, P. M. Rice, S. X. Wang and G. Li, *J. Am. Chem. Soc.*, 2003, **126**, 273-279.
56. S. H. Noh, W. Na, J. T. Jang, J. H. Lee, E. J. Lee, S. H. Moon, Y. Lim, J. S. Shin and J. Cheon, *Nano Lett.*, 2012, **12**, 3716-3721.
57. J. H. Lee, J. T. Jang, J. S. Choi, S. H. Moon, S. H. Noh, J. W. Kim, J. G. Kim, I. S. Kim, K. I. Park and J. Cheon, *Nat. Nanotechnol.*, 2011, **6**, 418-422.
58. J. Chen, X. Ye, S. J. Oh, J. M. Kikkawa, C. R. Kagan and C. B. Murray, *Acs Nano*, 2013, **7**, 1478-1486.
59. J. Cheon, J. I. Park, J. S. Choi, Y. W. Jun, S. Kim, M. G. Kim, Y. M. Kim and Y. J. Kim, *Proc. Natl. Acad. Sci. U. S. A.*, 2006, **103**, 3023-3027.
60. S. Sun, *Adv. Mater.*, 2006, **18**, 393-403.
61. M. Chen, J. Kim, J. P. Liu, H. Fan and S. Sun, *J. Am. Chem. Soc.*, 2006, **128**, 7132-7133.
62. M. Chen, J. P. Liu and S. Sun, *J. Am. Chem. Soc.*, 2004, **126**, 8394-8395.
63. S. W. Chou, C. L. Zhu, S. Neeleshwar, C. L. Chen, Y. Y. Chen and C. C. Chen, *Chem. Mater.*, 2009, **21**, 4955-4961.
64. C. Wang, Y. L. Hou, J. M. Kim and S. H. Sun, *Angew. Chem. Int. Ed.*, 2007, **46**, 6333-6335.
65. J. Kim, C. Rong, J. P. Liu and S. Sun, *Adv. Mater.*, 2009, **21**, 906-909.
66. C. b. Rong, D. Li, V. Nandwana, N. Poudyal, Y. Ding, Z. L. Wang, H. Zeng and J. P. Liu, *Adv. Mater.*, 2006, **18**, 2984-2988.
67. J. Kim, C. Rong, Y. Lee, J. P. Liu and S. Sun, *Chem. Mater.*, 2008, **20**, 7242-7245.
68. D. C. Lee, F. V. Mikulec, J. M. Pelaez, B. Koo and B. A. Korgel, *J. Phys. Chem. B*, 2006, **110**, 11160-11166.
69. Y. Piao, J. Kim, H. Bin Na, D. Kim, J. S. Baek, M. K. Ko, J. H. Lee, M. Shokouhimehr and T. Hyeon, *Nat. Mater.*, 2008, **7**, 242-247.
70. H. Zeng, J. Li, J. P. Liu, Z. L. Wang and S. H. Sun, *Nature*, 2002, **420**, 395-398.
71. H. Zeng, J. Li, Z. L. Wang, J. P. Liu and S. H. Sun, *Nano Lett.*, 2004, **4**, 187-190.
72. G. S. Chaubey, V. Nandwana, N. Poudyal, C. B. Rong and J. P. Liu, *Chem. Mater.*, 2008, **20**, 475-478.
73. A. Figuerola, A. Fiore, R. Di Corato, A. Falqui, C. Giannini, E. Micotti, A. Lascialfari, M. Corti, R. Cingolani, T. Pellegrino, P. D. Cozzoli and L. Manna, *J. Am. Chem. Soc.*, 2008, **130**, 1477-1487.
74. F. Liu, J. Zhu, W. Yang, Y. Dong, Y. Hou, C. Zhang, H. Yin and S. Sun, *Angew. Chem. Int. Ed.*, 2014, **53**, 2176-2180.
75. T. Teranishi, A. Wachi, M. Kanehara, T. Shoji, N. Sakuma and M. Nakaya, *J. Am. Chem. Soc.*, 2008, **130**, 4210-4211.
76. Y. Yu, K. Sun, Y. Tian, X. Z. Li, M. J. Kramer, D. J. Sellmyer, J. E. Shield and S. Sun, *Nano Lett.*, 2013, **13**, 4975-4979.
77. Y. Hou, Z. Xu, S. Peng, C. Rong, J. P. Liu and S. Sun, *Adv. Mater.*, 2007, **19**, 3349-3352.
78. H. W. Zhang, S. Peng, C. B. Rong, J. P. Liu, Y. Zhang, M. J. Kramer and S. H. Sun, *J. Mater. Chem.*, 2011, **21**, 16873-16876.
79. P. K. Deheri, S. Shukla and R. V. Ramanujan, *J. Solid State Chem.*, 2012, **186**, 224-230.
80. P. K. Deheri, V. Swaminathan, S. D. Bhame, Z. Liu and R. V. Ramanujan, *Chem. Mater.*, 2010, **22**, 6509-6517.
81. G. S. Chaubey, N. Poudyal, Y. Liu, C. Rong and J. P. Liu, *J. Alloys Compd.*, 2011, **509**, 2132-2136.
82. C. Yang, L. Jia, S. Wang, C. Gao, D. Shi, Y. Hou and S. Gao, *Sci. Rep.*, 2013, **3**, 3542.
83. D. J. Sellmyer, *Nature*, 2002, **420**, 374-375.
84. C. B. Rong, V. Nandwana, N. Poudyal, J. P. Liu, M. E. Kozlov, R. H. Baughman, Y. Ding and Z. L. Wang, *J. Appl. Phys.*, 2007, **102**, 02908.
85. C. B. Rong, Y. Zhang, N. Poudyal, X. Y. Xiong, M. J. Kramer and J. P. Liu, *Appl. Phys. Lett.*, 2010, **96**, 102513.
86. C. B. Rong, N. Poudyal, X. B. Liu, Y. Zhang, M. J. Kramer and J. P. Liu, *Appl. Phys. Lett.*, 2012, **101**, 152401.
87. L. Y. Zheng, B. Z. Cui, L. X. Zhao, W. Li, M. G. Zhu and G. C. Hadjipanayis, *J. Nanopart. Res.*, 2012, **14**, 1129.
88. E. Kita, T. Oda, T. Kayano, S. Sato, M. Minagawa, H. Yanagihara, M. Kishimoto, C. Mitsumata, S. Hashimoto, K. Yamada and N. Ohkohchi, *J. Phys. D: Appl. Phys.*, 2010, **43**, 474011.
89. R. Hergt, S. Dutz, R. Muller and M. Zeisberger, *J. Phys.-Condes. Matter*, 2006, **18**, S2919-S2934.
90. S. Mornet, S. Vasseur, F. Grasset and E. Duguet, *J. Mater. Chem.*, 2004, **14**, 2161-2175.
91. A. Jordan, R. Scholz, P. Wust, H. Fahling and R. Felix, *J. Magn. Magn. Mater.*, 1999, **201**, 413-419.
92. R. E. Rosensweig, *J. Magn. Magn. Mater.*, 2002, **252**, 370-374.
93. D. C. Jiles and D. L. Atherton, *J. Magn. Magn. Mater.*, 1986, **61**, 48-60.
94. J. P. Fortin, C. Wilhelm, J. Servais, C. Menager, J. C. Bacri and F. Gazeau, *J. Am. Chem. Soc.*, 2007, **129**, 2628-2635.
95. R. Kappiyoor, M. Liangruksa, R. Ganguly and I. K. Puri, *J. Appl. Phys.*, 2010, **108**, 094702.
96. B. Mehdaoui, A. Meffre, J. Carrey, S. Lachaize, L. M. Lacroix, M. Gougeon, B. Chaudret and M. Respaud, *Adv. Funct. Mater.*, 2011, **21**, 4573-4581.
97. M. S. Seehra, V. Singh, P. Dutta, S. Neeleshwar, Y. Y. Chen, C. L. Chen, S. W. Chou and C. C. Chen, *J. Phys. D: Appl. Phys.*, 2010, **43**, 145002.
98. J. T. Jang, H. Nah, J. H. Lee, S. H. Moon, M. G. Kim and J. Cheon, *Angew. Chem. Int. Ed.*, 2009, **48**, 1234-1238.
99. L. M. Lacroix, N. F. Huls, D. Ho, X. L. Sun, K. Cheng and S. H. Sun, *Nano Lett.*, 2011, **11**, 1641-1645.
100. L. M. Lacroix, R. B. Malaki, J. Carrey, S. Lachaize, M. Respaud, G. F. Goya and B. Chaudret, *J. Appl. Phys.*, 2009, **105**, 023911.
101. A. Meffre, B. Mehdaoui, V. Kelsen, P. F. Fazzini, J. Carrey, S. Lachaize, M. Respaud and B. Chaudret, *Nano Lett.*, 2012, **12**, 4722-4728.

TOC

This review summarizes recent progress in chemical synthesis and applications of exchange-coupled nanocomposites.